Research Article | Vol. 2, No. 3 / 15 March 2019 / OSA Continuum 797


# Raman and quantitative-phase microscope with counter-propagating beams demonstrated on HeLa cells

ALEJANDRO DIAZ TORMO,[1,*] DMITRY KHALENKOW,[2] ANDRE G. SKIRTACH,[2] AND NICOLAS LE THOMAS[2]

[1] *Photonics Research Group, Department of Information Technology, Ghent University - imec & Center for Nano- and Biophotonics, Ghent University, Belgium*
[2] *Department of Molecular Biotechnology, Ghent University, Ghent, Belgium*
[*] *alejandro.diaztormo@ugent.be*

**Abstract:** Raman spectroscopy probes the chemical composition of biological samples with sub-micron resolution, rendering it a powerful tool in the diagnosis of several diseases and the study unstained biological samples. However, the weak Raman signal leads to long acquisition times, unsuited to study dynamical processes or large samples. Quantitative phase microscopy can speed up the diagnosis, provide complementary data, and potentially link the Raman fingerprint of the sample with corresponding refractive indices. Here we demonstrate a $4\pi$ microscope that records both the Raman and quantitative phase information from the same sample spot.



## 1. Introduction

Illnesses can present themselves in many different forms. Changes in the morphology, chemical composition and biophysical parameters, such as matter density and cell dry mass, provide different windows through which the illnesses can be understood and diagnosed [1–5].

The chemical composition of the sample can be probed by Raman spectroscopy in a noninvasive way and without the need of extrinsic labels. In the biomedical field, Raman spectroscopy has already been employed to diagnose cancer [1,2], monitor blood glucose [3], differentiate cell lines [4] and sub-compartments [6], and many other applications.

To monitor morphology and biophysical parameters, Quantitative Phase Microscopy (QPM) can be employed. It has been used in the diagnosis of cancer [5] and in cell pathology studies [7–10].

These two techniques, Raman and QPM, have been used before to complement other microscopy techniques, for instance, Raman spectroscopy has been combined with fluorescence microscopy [11] and optical coherence tomography [12]. They have also been combined together. In [13,14] QPM preselects red blood cells potentially infected by malaria to be carefully examined with Raman spectroscopy. A typical diagnosis would be based on a slow Raman scan across the whole sample, but using full-field QPM makes the diagnosis orders of magnitude faster while maintaining the necessary specificity to diagnose malaria. In [15] the authors make an extended study of the relationship between ultraviolet exposure and skin cancer using both modalities, QPM and Raman spectroscopy.

In the aforementioned works a completely different setup for each modality was used [15], a different optical path [13,14] or even a different wavelength [16,17]. This explains the need for algorithms to match the different magnifications, field of views, translations, rotations and dispersion effects of both images. Moreover, different aberrations and resolutions are completely disregarded.

In this paper we propose a microscope with two complementary modalities —Raman and Quantitative Phase Microscopy— to study cell processes from two different points of view

#355175 https://doi.org/10.1364/OSAC.2.000797
Journal © 2019 Received 12 Dec 2018; revised 13 Feb 2019; accepted 13 Feb 2019; published 12 Mar 2019

OSA CONTINUUM

simultaneously. It uses a common-path point-scanning approach for both modalities where the same laser beam serves two purposes: Raman pump and probe for the quantitative phase measurement. Consequently, we obtain an inherent match between data sets. The aberrations and resolution are the same, and the data are taken from the exact same sample spot without the need of any post-processing to match both images.

Importantly, the quantitative phase obtained is free of any phase wrapping constraints in a dynamic range of more than 200 radians while being compatible with the Raman modality of the microscope. This microscope allows correlating the Raman and quantitative phase information [16] from the same spot of a HeLa cell, which has the potential to become a new tool in the diagnosis of disease.

## 2. Experimental setup and methods

The microscope is based on two counter-propagating beams, focused on the same spot by two objective lenses. This configuration is also known as $4\pi$ microscopy, and we used it previously for $4\pi$ Raman experiments in [18]. The point spread function of the microscope was characterized in [19], yielding a main lobe of 230 nm full-width-half-maximum.

Figure 1 shows the optical scheme of the quantitative phase and Raman microscope. The Raman signal, collected by a 100 $\mu$m core-diameter multimode fiber, is measured by a spectrometer (UHTS 300 with a −70 °C cooled CCD camera, ANDOR iDus 401 BR-DD and a grating with 300 grooves/mm), and the phase signal by a photodetector (Thorlabs SM1PD1A). The beam from a single-mode 785 nm laser diode (Toptica XTRA II) is split into two paths. One path is connected to the top part of a Raman microscope (WITec alpha300 upgraded to add inverted access), and the other to the bottom thereof. The total laser power measured after the coupling into a monomode polarization maintaining fiber is 260 mW.

The counter-propagating beams interfere at the sample plane forming a $4\pi$ point spread function and acting as the Raman pump. The transmitted beam through the sample and a partial reflection from the bottom beam, both indicated by red arrows, undergo a phase shift $\phi_T$ and $\phi_R$, respectively. The sample introduces an additional optical length $\phi_{sample}$ present in the photodetector signal $\cos(\phi_T + \phi_{sample} - \phi_R - \phi_f)$ will be defined later. The isolator in the interferometer filters out the transmitter beam from bottom to top, and the reflection from the top beam at the partial reflector. This results in a simpler two-beam interferogram instead of having to consider four beams.

Different objective lenses were used in the top (Zeiss, Water immersion Plan-Apochromat M27 63x/1.0NA) and bottom (Nikon, Plan Fluor DIC 20x0.5NA) sides of the sample. Ideally the same high NA objectives would be used on both sides to get the smallest PSF possible. Here we use a lower NA on the bottom side for two main practical reasons. First, a lower NA yields a larger focal volume and therefore it maintains a better alignment with the top objective when subjected to thermal drifts of the stages. Second, its long working distance is needed to go through relatively thick substrates, 120 $\mu$m of $CaF_2$ in our case. The optical powers reaching the back-aperture of the top and bottom objectives are 35 and 58 mW, respectively. The asymmetry between arms is due to the 2.2 dB losses of the isolator in the interferometer, and it is partially compensated by the different confocal volumes of the objectives.

Depending upon whether the Proportional-Integral-Derivative controller (PID) is turned on or off we can have two functional regimes. When the PID is turned off the system is not stabilized, i.e., the setup is on free-running mode. We use input channel 1 of the oscilloscope to directly observe the signal from the photodetector. Following the model for the detector signal $V = O_f + A \cdot cos(\phi)$ we can now calculate the voltage corresponding to any desired phase shift between pump beams at the partial reflector plane. As the thermal phase fluctuations evolve and change $\phi$ over a range bigger than $\pi$, the amplitude value $A$ of the cosine and the offset $O_f$ can be obtained.

OSA CONTINUUM

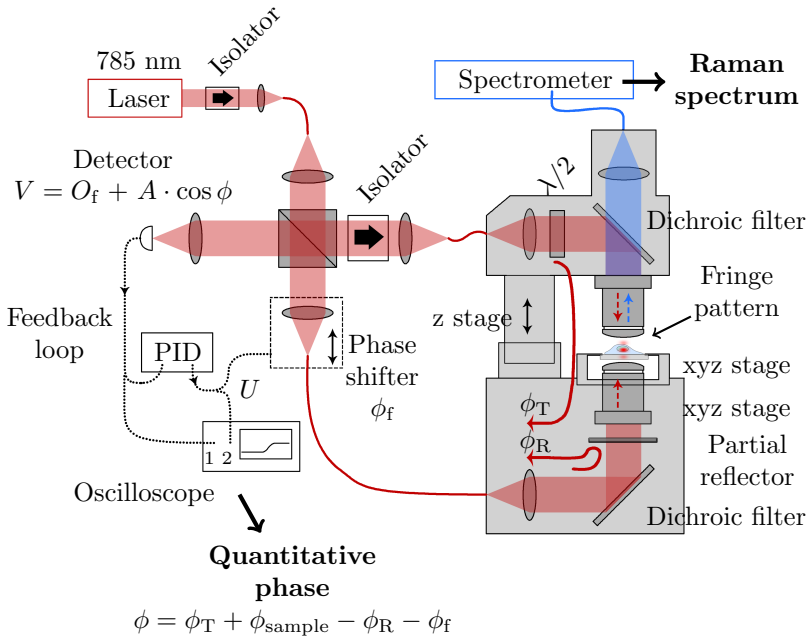


**Fig. 1.** Schematic of the Raman and quantitative phase microscope. The optical path length of the transmitted beam and the partially reflected beam from the partial reflector are indicated a $\phi_T$ and $\phi_R$, respectively. The red solid arrows indicate the beams that will interfere at the detector to produce the signal $V = O_f + A \cdot \cos(\phi_T + \phi_{sample} - \phi_R - \phi_f)$ that depends on the phase shift between transmitted and reflected pump beams, including the influence of the sample $\phi_{sample}$ and phase shifter $\phi_f$. The Raman spectra are obtained by the spectrometer and the quantitative phase by the detector connected to a feedback loop.

We can speed up this process by forcing some phase noise into the system through the phase shifter (translation stage).

For the stable regime the PID is turned on. We then set the appropriate PID parameters (proportional, integral and derivative gains, and internal setpoint) to stabilize the system at the chosen voltage. For the following calibration experiments the specific voltage (phase) value is not relevant as long as the system can be stabilized, but it will be relevant for the experiments with cells shown later. The role of the PID is to drive the phase shifter in such a way that its input, the detector signal, is kept fixed at the desired voltage, and it does so by driving the translation stage, referenced to as *phase shifter*, that moves one of the collimating lenses to change the optical length in one of the interferometer arms.

It is noteworthy that we do not access the phase shift induced by the sample in a conventional way, relying on the cosine term of an interferogram. Any change of the phase shift at the sample plane can be traced back in the form of the voltage $U$ driving the phase shifter, corresponding to a phase shift referred to as $\phi_f$. Once the environmental phase noise is averaged out, the driving voltage $U$ is directly proportional to $\phi_{sample}$ as the PID ensures that any change on $\phi_{sample}$ will be compensated by changing $\phi_f$. There is no sinusoidal term involved in the measurement and, hence, the phase values obtained in this manner are unaffected by phase wrapping.

OSA CONTINUUM

To isolate $\phi_{\text{sample}}$ from the detector signal we currently have to remove the environmental low-frequency phase noise in the system by taking 25 measurements and averaging them, which sets the phase scan time.

In this proof of principle experiment the speed of a single phase line-scan is limited by the speed at which the software is able to communicate with the piezo stage used to scan the sample. It currently takes 40 seconds to acquire the 70-point scans of biological samples shown later in Fig. 3. Connecting a ramp generator directly to the piezo stage would spare the communication with the controller and, therefore, it would increase the measurement speed.

The quantitative phase, as well as the Raman molecular fingerprints, are measured in a confocal manner. This confocality in the QPM modality, although key to obtaining the advantages described above, comes at the price of losing its conventional full-field capability.

The polarization of both arms of the interferometer must be the same to obtain coherent interference at the sample plane. The laser output is linearly polarized, and it is kept so by using polarization maintaining fibers. A half wave plate present in the top part of the microscope turret rotates the linear polarization of the top beam in order to match the bottom beam.

We currently obtain the Raman and the quantitative phase in subsequent scans. A completely simultaneous scan of both modalities is hindered by the phase noise in the fibers induced by environmental fluctuations [20]. The optical fibers play the role of the pinhole, as part of the confocal microscope, but they are not strictly necessary. They connect the interferometer with the commercial microscope turret, but it could be possible to substitute them by actual pinholes and enclose all the setup inside the same turret or microscope stand. Thus, an approach to speed up the measurements would be to remove the source of phase noise, the fibers, leading to truly simultaneous Raman and QPM of the same spot of the sample.

The phase shifts measured by the phase modality are quantitative only after a pre-calibration step. In Fig. 2 the results of this calibration step are shown. Figure 2(a) shows a visible top-view image of the sample used, consisting of an ARP (electron beam resist) nanolayer on top of a 120 $\mu$m $CaF_2$ substrate. We selected a Raman grade $CaF_2$ because of its low fluorescence background. The ARP was etched away after a lithographic process to open a window through which the $CaF_2$ substrate can be seen. In Fig. 2(b) the height of the ARP nanolayer was measured with a profilometer (Dektak), yielding 200 $\pm$1 nm.

While scanning the sample with our microscope we monitor the output voltage of the feedback loop that drives the phase-shifter. In Fig. 2(b) we see that 0.18 V on the phase-shifter compensate the phase shift induced by the ARP layer. The refractive index of ARP given by the manufacturer is 1.56 at the laser wavelength. For the open window the reflection happens at the $CaF_2$ interface. However, the part covered with ARP has two interfaces, air-ARP and ARP-$CaF_2$, leading to interference effects that need to be considered. A transfer matrix calculation including these effects yields an extra phase shift of $0.82\lambda$, or equivalently 3.87 radians. This calculation assumes normal incidence but a Finite-Difference Time-Domain simulation could be more precise by considering the entire range of angles given by the objective lenses. In the worst case scenario, for the highest incidence angle given by the objective lenses, we estimate a higher total phase shift of 4.42 radians.

We conclude that a phase shift of 3.87 radians corresponds to a driving voltage of 0.18 V, leading to the calibration coefficient 21.5 rad/V that we will use to obtain the quantitative phase. Regarding the phase shift dynamic range, the limiting factor is given by the 10 V range of the feedback electronics output, so given the previous coefficient it results in more than 200 rad as long as the phase gradient of the sample are smooth and no steps bigger than $2\pi$ are present.

OSA CONTINUUM

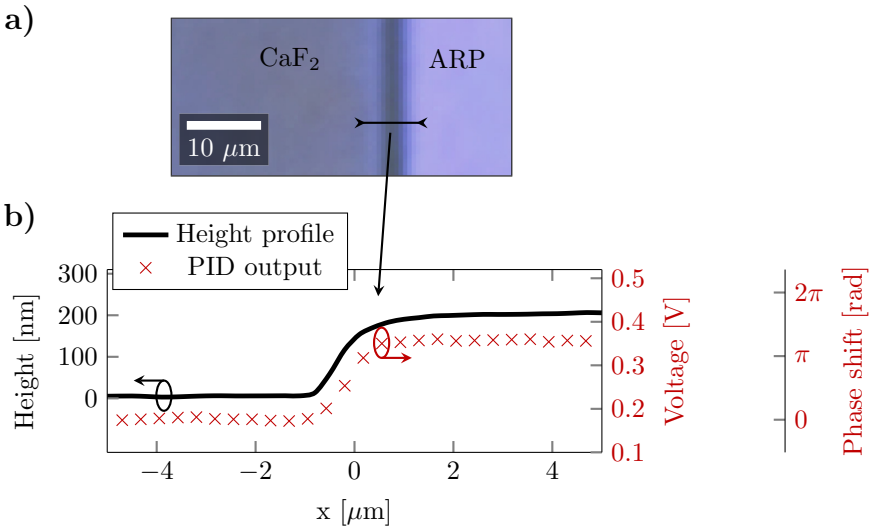


**Fig. 2.** Phase calibration experiment using an ARP nanolayer on top of a 120 $\mu$m $CaF_2$ substrate. Part of the ARP was lithographically removed to access the $CaF_2$ directly. **a)** Visible image. **b)** Nanolayer height obtained with a profilometer and PID output voltage, which is proportional to the phase shift induced by the sample. These data are obtained from the part of the sample indicated in a) with a black line.

## 3. HeLa cell experiment

The results of the Raman and quantitative phase line scans of a fixed HeLa cell are shown in Fig. 3. The cells were fixed for 10 min with 4% formaldehyde (4078-9001, Klinipath) and washed 3 times with HBSS solution (14025050, ThermoFisher). The commercial microscope turret allows us to easily remove the top dichroic filter and to choose a different optical path to work as a bright-field microscope (white light source and camera not shown on the schematic of Fig. 1). In order to have a visual aid, a bright-field image of the cell was taken right before the scans on the right side of the figure. A Raman spectrum from the nucleus of the cell is shown below the visible image. This spectrum is selected from all the full Raman spectra taken for the scans. The exact spot from which it was obtained is indicated with a blue cross in the bright field image and in the corresponding scan. The 784 $cm^{-1}$ peak corresponds to a DNA band and is chosen for the Raman scans shown on the right side of the figure.

For both modalities, Raman and quantitative phase, we took 70 measurements while scanning the sample in the $x$ direction, where each Raman spectrum took 6 seconds to be acquired. Using the calibration factor obtained with the ARP sample we additionally obtained the quantitative phase shift induced by different parts of the HeLa cell. The maximum value of $\pi/2$ radians is in agreement with the literature [21,22], which is in the order of a few radians for this kind of cells.

The first scan labeled **a** focuses on the substrate and a barely visible particle (indicated with an arrow) of 1.3 $\mu$m diameter, giving an idea of the microscope sensitivity. Although the particle is masked by the noise in the entire Raman spectrum, a significant bump is detected by the quantitative phase modality.

Two more line scans, **b** and **c**, are shown, one of them going through part of the HeLa cell with cytoplasm and small organelles, and the other mostly going through the nucleus. In general, it can be seen that both modalities show a high degree of correlation. This is expected as the presence of a higher number of cell molecules leads to a signal increase in both cases.

OSA CONTINUUM

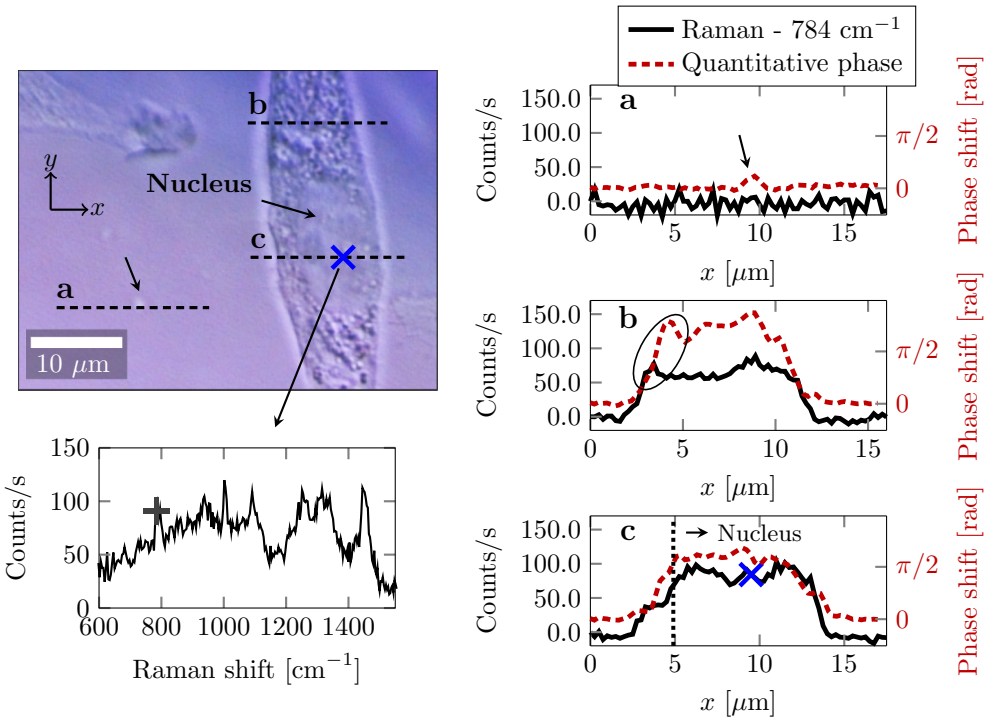


**Fig. 3.** Raman and quantitative phase scans of a fixed HeLa cell. On the left, bright-field image and a Raman spectrum of the cell where the peak of interest at 784 $cm^{-1}$ is indicated with a cross. On the right, Raman and quantitative phase scans of three different spots of the sample indicated with dashed lines on the visible image. The presence of a small particle in the fist scan **a** is highlighted with an arrow. The evolution of the Raman fingerprint in the horizontal direction $x$, namely the peak at 784 $cm^{-1}$, is plotted in black. The corresponding Raman counts per second are indicated on the left vertical axis. The quantitative phase of the respective scans is indicated with dashed red curves and are linked to the vertical axis on the right.

Some parts of the scans show differences between the Raman and phase curves, mostly visible at the edge of the cell. The most clear difference, marked with an ellipse, lies on the scan **b** around $x = 4\mu$m and we suspect it is due to edge effects that need further investigation.

Scan **c** shows a slightly more intense Raman signal compared to scan **b**, expected from the DNA Raman band analyzed. However, the setup in its current state is prone to stage thermal drifts between scans, which can affect the intensities of the different scans. We realigned the objective lenses at the beginning of scans **a**, **b** and **c** in order to reduce them. This realignment could be avoided enclosing all the optical components inside the same microscope turret, which would improve the thermal isolation of the setup. The quantitative phase scan is more robust against the misalignment because the substrate is reset as the 0 rad reference for every scan.

Looking at the visible image, there is a small part of cytoplasm at the beginning of scan **c** before it reaches the nucleus of the cell. The quantitative phase information does not show a clear difference between both parts. Conversely, the Raman signal at the selected peak is higher at the cytoplasm part, which can be used to separate both contributions and shows how both modalities can complement each other in a practical application.

When the data show a high degree of correlation between modalities, using QPM suffices to diagnose a given disease. Under this condition, using only QPM could potentially speed up the

OSA CONTINUUM

process since the Raman measurements pose the speed limiting factor. In the opposite case the uncorrelated data show that different molecules within the sample have different refractive indices. In cell studies this will allow estimating the refractive index of the different sub-components from a Raman measurement.

## 4. Conclusion

Raman microscopy is a powerful tool in the diagnosis of several diseases and, more in general, to study unstained biological samples. Despite its potential, the slow acquisition of data hinders its applicability in the study of dynamical processes or large sample areas. Here we discussed how a quick quantitative phase microscopy can speed up, substitute or complement the slow molecular Raman imaging process.

In its current state the speed of the QPM modality is limited by the thermal phase fluctuations that need to be averaged out with several scans of the same spots and the communication with the scanning piezo stage. Both are solvable issues. Enclosing all the optics inside the same microscope turret in a compact way could potentially render the phase stabilization unnecessary, although a phase shifter would still be necessary to adjust the phase shift between beams at the sample plane. Regarding the communication with the scanning piezo stage, a ramp generator could be directly connected to it, instead of slowly communicating through a PC. Implementing these setup modifications would mean the QPM speed would only be limited by the sensitivity and speed of the photodetector, potentially reaching speeds for scans like the ones presented here in the order of 100 milliseconds or less instead of the current ~17 minutes.

Moreover, the quantitative phase modality of the proposed microscope is unconventional because it does not rely on the measurement of the sinusoidal term of an interferogram. Therefore, it does not suffer from phase-wrapping issues and does not require to unwrap the phase in a post-processing algorithm. The phase shift of the sample is directly proportional to the experimental observable, i.e. the feedback voltage, over a 200 radians dynamic range.

The method could also be used to study the correlation between composition of inner structures within living organisms and their refractive index.

To conclude, we demonstrated that the $4\pi$ quantitative phase and Raman microscope discussed in this work offers several advantages compared to previous studies in terms of resolution and, most importantly, in terms of the inherent alignment between modalities.

## Funding

Bijzonder Onderzoeksfonds (BOF) (BOF14/IOP/003, BAS094-18); Fonds Wetenschappelijk Onderzoek (FWO) (G043219N).

## Acknowledgments

This research is supported by the Special Research Fund (BOF) of Ghent University (BOF14/IOP/003). AGS also acknowledges support by BOF-UGent (BAS094-18) and FWO-Vlaanderen (G043219N).

## Disclosures

The authors declare that there are no conflicts of interest related to this article.

## References

1. L. A. Austin, S. Osseiran, and C. L. Evans, "Raman technologies in cancer diagnostics," Analyst **141**(2), 476–503 (2016).
2. S. K. Paidi, A. Rizwan, C. Zheng, M. Cheng, K. Glunde, and I. Barman, "Label-free raman spectroscopy detects stromal adaptations in premetastatic lungs primed by breast cancer," Cancer Res. **77**(2), 247–256 (2017).
3. R. Pandey, S. K. Paidi, T. A. Valdez, C. Zhang, N. Spegazzini, R. R. Dasari, and I. Barman, "Noninvasive monitoring of blood glucose with raman spectroscopy," Acc. Chem. Res. **50**(2), 264–272 (2017).

OSA CONTINUUM


4. R. J. Swain, S. J. Kemp, P. Goldstraw, T. D. Tetley, and M. M. Stevens, "Assessment of cell line models of primary human cells by raman spectral phenotyping," Biophys. J. **98**(8), 1703–1711 (2010).
5. P. Wang, R. Bista, R. Bhargava, R. E. Brand, and Y. Liu, "Spatial-domain low-coherence quantitative phase microscopy for cancer diagnosis," Opt. Lett. **35**(17), 2840–2842 (2010).
6. A. Yashchenok, A. Masic, D. Gorin, B. S. Shim, N. A. Kotov, P. Fratzl, H. Möhwald, and A. Skirtach, "Nanoengineered colloidal probes for raman-based detection of biomolecules inside living cells," Small **9**(3), 351–356 (2013).
7. B. Rappaz, E. Cano, T. Colomb, J. Kuhn, C. D. Depeursinge, V. Simanis, P. J. Magistretti, and P. P. Marquet, "Noninvasive characterization of the fission yeast cell cycle by monitoring dry mass with digital holographic microscopy," J. Biomed. Opt. **14**(3), 034049 (2009).
8. K. J. Chalut, A. E. Ekpenyong, W. L. Clegg, I. C. Melhuish, and J. Guck, "Quantifying cellular differentiation by physical phenotype using digital holographic microscopy," Integr. Biol. **4**(3), 280–284 (2012).
9. L. Kastl, M. Isbach, D. Dirksen, J. Schnekenburger, and B. Kemper, "Quantitative phase imaging for cell culture quality control," Cytometry, Part A **91**(5), 470–481 (2017).
10. K. Lee, K. Kim, J. Jung, J. Heo, S. Cho, S. Lee, G. Chang, Y. Jo, H. Park, and Y. Park, "Quantitative phase imaging techniques for the study of cell pathophysiology: from principles to applications," Sensors **13**(4), 4170–4191 (2013).
11. H.-J. van Manen, Y. M. Kraan, D. Roos, and C. Otto, "Single-cell raman and fluorescence microscopy reveal the association of lipid bodies with phagosomes in leukocytes," Proc. Natl. Acad. Sci. USA **102**(29), 10159–10164 (2005).
12. C. Patil, J. Kalkman, D. J. Faber, J. S. Nyman, T. G. van Leeuwen, and A. Mahadevan-Jansen, "Integrated system for combined raman spectroscopy-spectral domain optical coherence tomography," J. Biomed. Opt. **16**(1), 011007 (2011).
13. J. W. Kang, N. Lue, C.-R. Kong, I. Barman, N. C. Dingari, S. J. Goldfless, J. C. Niles, R. R. Dasari, and M. S. Feld, "Combined confocal raman and quantitative phase microscopy system for biomedical diagnosis," Biomed. Opt. Express **2**(9), 2484–2492 (2011).
14. J. Klossa, B. Wattelier, T. Happillon, D. Toubas, L. de Laulanie, V. Untereiner, P. Bon, and M. Manfait, "Quantitative phase imaging and raman micro-spectroscopy applied to malaria," Diagn. Pathol. **8**(S1), S42 (2013).
15. S. Singh, S. Kang, J. W. Kang, P. T. So, R. R. Dasari, Z. Yaqoob, and I. Barman, "Label-free characterization of ultra violet-radiation-induced changes in skin fibroblasts with raman spectroscopy and quantitative phase microscopy," Sci. Rep. **7**(1), 10829 (2017).
16. N. Pavillon, A. J. Hobro, and N. I. Smith, "Cell optical density and molecular composition revealed by simultaneous multimodal label-free imaging," Biophys. J. **105**(5), 1123–1132 (2013).
17. N. Pavillon and N. I. Smith, "Implementation of simultaneous quantitative phase with raman imaging," EPJ Tech. Instrum. **2**(1), 5 (2015).
18. A. D. Tormo, D. Khalenkow, K. Saurav, A. G. Skirtach, and N. Le Thomas, "Superresolution $4\pi$ raman microscopy," Opt. Lett. **42**(21), 4410–4413 (2017).
19. A. D. Tormo, D. Khalenkow, A. G. Skirtach, and N. Le Thomas, "$4\pi$ microscopy immune to sample-induced dephasing," in *2018 IEEE Photonics Conference (IPC)*, (IEEE, 2018), pp. 1–2.
20. R. E. Bartolo, A. B. Tveten, and A. Dandridge, "Thermal phase noise measurements in optical fiber interferometers," IEEE J. Quantum Electron. **48**(5), 720–727 (2012).
21. B. Bhaduri, H. Pham, M. Mir, and G. Popescu, "Diffraction phase microscopy with white light," Opt. Lett. **37**(6), 1094–1096 (2012).
22. D. Roitshtain, N. A. Turko, B. Javidi, and N. T. Shaked, "Flipping interferometry and its application for quantitative phase microscopy in a micro-channel," Opt. Lett. **41**(10), 2354–2357 (2016).